FAST DETECTION OF PROSTATE MALIGNANT TISSUE BY MULTIPULSED LAER-INDUCED BREAKDOWN SPECTROSCOPY (LIBS)

DETECCIÓN RÁPIDA DE TEJIDO MALOGNO EN LA PRÓSTATA EMPLEANDO LA TÉCNICA DE RUPTURA INDICIDA POR LÁSER ILIBS) EN RÉGIMEN MULTIPULSO

A. Ponce[a], T. Flores[a†] and L. Ponce[a,b]

a) Onteko LLC, 9924 Alexanders Ridge Dr., Olive Branch, MS 38654, USA
b) Saint Petersburg Electrotechnical University, Professora Popova St 5, 197376 St.Petersburg, Russia; manjuary@gmail.com[†]
† corresponding author

We evaluate the use of laser-induced breakdown spectroscopy (LIBS) coupled with chemometric methods as a fast and simple technique for identifying diseased tissue in prostate cancer samples. The experimental setup consisted of a neodymium-doped yttrium aluminum garnet (Nd:YAG) laser in a burst-mode regime, with differing time delays for the spectrometer readings. To improve classification accuracy, principal component analysis (PCA) was coupled with neural analysis (NA), achieving a high identification accuracy of 97 %. It can be concluded that LIBS has the potential to serve as a technique for the detection and diagnosis of human prostate cancer.

Evaluamos el uso de la espectroscopía de ruptura inducida por láser (LIBS) acoplada con métodos quimiométricos como una técnica rápida y sencilla para identificar tejido enfermo en muestras de cáncer de próstata. El dispositivo experimental consistió en un láser de granate ytrio-aluminio dopado con neodimio (Nd:YAG) en modo de pulsos, con diferentes retardos temporales para las lecturas espectrométricas. Para mejorar la calidad de la clasificación, se acopló el análisis de componente principal (PCA) con análisis neural (NA), lográndose una gran precisión de identificación, del 97 %. Se concluye que el LIBS posee el potencial de servir como técnica para la detección y diagnóstico de cáncer de próstata humano.

I. INTRODUCTION

Early detection is one of the most important factors determining cancer survival rates, but it remains a challenge, even after extensive and continuous efforts. In many cases, diagnosis depends on the subjective analysis of a biopsy sample. Other commonly used techniques, such as computer tomography and magnetic resonance imaging, are expensive, time-consuming, and do not provide detailed information about the boundaries between the tumor and the normal tissue surrounding it, which is essential to minimize the trauma induced during surgical operation. Thus, the development of fast and reliable detection methods could considerably improve clinical outcomes.

Laser-induced breakdown spectroscopy (LIBS) is a technique that meets all the requirements mentioned in the previous paragraph [1]. It has a growing impact on and popularity in compositional analysis because of its portability, high speed, low cost, capability to perform close to immediate identification, and the fact that it does not require chemicals [2]. The technique involves short laser pulses capable of ablating a small amount of material, thereby creating plasma momentarily. An optical fiber collects a portion of the light emitted from the plasma and delivers it to a spectrometer. The captured spectra constitute a "fingerprint" associated with a sample's elemental composition.

Since the first published report on the use of LIBS for the detection of cancerous tissue in 2004 [3], several research groups have developed different novel approaches for this potential application. These include the LIBS-based immunoassay (Tag-LIBS) [4], direct analysis of samples through the combined use of LIBS and machine learning algorithms [5], and the use of frozen samples or in-vacuum detection [6].

In this work, we introduce a different experimental approach for the LIBS technique that involves using a laser with a controllable sequence of pulses to reduce the signal-to-noise ratio, thus improving detection, coupled with principal component analysis (PCA) and neural networks.

II. MATERIALS AND METHODS

Normal tissue and cancer samples were obtained from the US Biolab Biorepository (Washington, D.C., United States). The samples were prostate tissue microarrays (TMA) containing cores with pathologically diagnosed adenocarcinoma and the corresponding normal prostate tissue.

As shown in Fig. 1, each core was approximately 1.5 mm in diameter and 2-5 μm in thickness. In each array, 16 adenocarcinoma cores and 10 normal prostate tissue cores

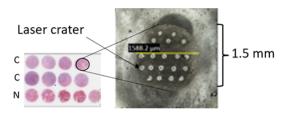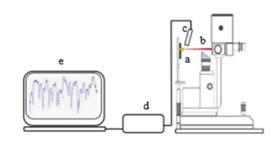were fixed with formalin on a microscope slide.

Figure 1. An illustration of the tissue microarray. C, Cancer samples; N, healthy reference samples. Right panel: the magnified image of one sample after being irradiated by several laser pulses.

III. LIBS EXPERIMENTAL SETUP

For the analysis, we used the "SLIT-LIBS" instrument supplied by Onteko LLC (Olive Branch, Mississippi, United States), which includes a laser that emits in a burst mode regime, as described below. In this device, the laser beam was coupled with the optical path of a slit-lamp microscope for better visualization of the samples.

A schematic representation of this setup is shown in Fig. 2. The pulsed (neodymium-doped yttrium aluminum garnet) Nd:YAG laser emits at a wavelength of 1,064 nm while working in a Q-switch regime, producing light pulses (shots) with an energy of up to 40 mJ at a frequency of 1 Hz. A low-power red laser was used to point where the Nd:YAG laser would irradiate, ablate the sample, and generate the plasma.

Each laser shot consisted of a train of up to three micro-pulses, each having a duration of 8 ns and an interval around 25 μs between each pulse, resulting in an overall shot duration of about 70-80 μs for the three-pulse train. The 2 mm in diameter laser beam was focalized using a 50 mm focal length lens, which produced a 44 μm spot diameter at the focal point. The laser ablation process induced the emission of light, which was collected by an optical fiber and delivered to a cross-Czerny-Turner spectrometer with a linear charged-coupled device (CCD) as a detector. The spectral resolution of the system was 0.3 nm, with a spectral range of 250-800 nm. The total reading time of the spectrometer was approximately 3.8 ms.

The use of a train of laser pulses instead of the typical single-pulse regime to improve the signal-to-noise ratio in LIBS has been reported in previous work [2]. The multi-pulse can be achieved in two ways:

A) If there is enough temporal separation between each laser pulse to avoid over-lapping with the plasma generated by the previous pulse, then the detected emission will be the sum of the plasma generated by the three pulses. To accomplish this result, the pulses must be separated by several dozen microseconds.

B) If the separation between pulses is just a few microseconds long, each new pulse will be partially absorbed by the plasma generated by the previous one. In this case, it is possible to re-excite the plasma, leading to a higher intensity of the

spectral peaks and improved detection.

Figure 2. A schematic of the experimental setup: a) sample, b) laser beam, c) detector, d) spectrometer, e) computer.

IV. EXPERIMENT DESCRIPTION

For the spectra collection, a tissue microarray slide was placed over a platform located directly in front of the laser emission source. Our instrument allowed visual observation of the sample through a microscope with a magnification of up to 40X and collimation of the laser over the desired spot on the sample using a micrometric xyz stage.

This setup allowed us to perform the spectral measurements from several spots in each tissue core.

Once each core ran out of fresh available surface, we moved on to the next. Fig. 3A shows a representative example of a crater created as a result of the laser pulse. The crater shown has a diameter of 154 μm and depth of 2.34 μm. The image and crater profile were obtained with a Lext OLS5000 confocal microscope from Olympus (Waltham, Massachusetts, USA). The central part of the Gaussian beam also slightly ablated the glass substrate in the center of the crater, as shown in the 3D image in Fig. 3B.

To calculate the total mass extracted by the pulse, the geometry of the crater was approximated as a cylinder with a diameter of 150 μm and a depth of 2.3 μm. Then, for a prostate tissue density of 0.98 g/mL [7], the ablated mass will be less than 41 ng per crater.

Assuming that a LIBS device is used as an alternative to a traditional prostate biopsy analyzing 10 different areas and taking 50 spectra in each area, the total extracted tissue would amount to around 0.02 mg. This is considerably less than a traditional biopsy, which typically requires close to 200 mg of tissue [8]. This represents an important advantage when considering LIBS as a potential technique for cancer biopsies.

In Fig. 3B, the orange lines show between which points it is measured, while the dotted blue lines indicate the measured values. For example, the blue dotted line above indicates 154 μm for the diameter of the crater. The vertical dotted blue line located on the left indicates the depth of most of the crater base, which is 2.34 μm. Finally, the blue dotted line on the far

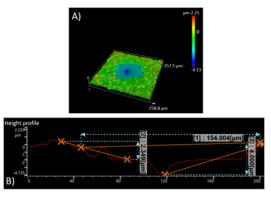right indicates the maximum depth of the crater of 4 μm.

Figure 3. A) A representative 3D image of the laser crater. B) The depth profile of the laser crater.

Each laser pulse generates plasma, and its emitted light is captured through an optic fiber, which delivers it into a USB400 spectrometer. In total, 400 spectra were captured, with 100 spectra for cancer tissue and 100 for normal tissue repeated at 2 μs and 10 μs delays where the delay refers to the start of the spectrometer reading with respect to the laser pulse. The spectra shown in Fig. 4 (top panel) are the averages of each group.

V. RESULTS AND DISCUSSION

Fig. 4 (top panel) shows the spectra of healthy and cancer tissue samples captured with a 2 μs delay, as well as the spectra resulting from the subtraction between the two. With this delay setting, significant electronic background noise can be observed. This came from the first two micropulses and is contributing to the differentiation between normal and cancer samples, possibly due to the differences in absorption of the laser radiation between the plasma produced by healthy and cancer tissue. Additionally, several elemental peaks contributed to the difference, most notably Fe, Ca, and Na.
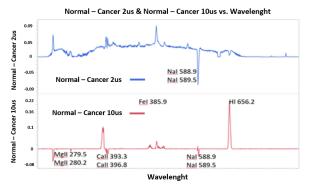

Figure 4. Top panel: LIBS spectral for the difference spectra (blue) with a time delay of 2 μs. Bottom panel: LIBS spectra for the differ-ence spectra (red) with a time delay of 10 μs.

The spectra captured using a time delay of 10 μs (Fig. 4, bottom panel) show characteristic lines that correspond to plasma species whose lifetime must be longer than 10 μs. For this case, we had no bremsstrahlung, as the spectrometer

started recording after the electronic background for the last pulse had faded. In the difference spectra, several lines were not distinguishable with a delay of 2 μs, probably because some of the less intense lines were masked by the electronic background.

As with the 2 μs spectra, the difference spectrum for the 10 μs time delay was obtained by subtracting the averages of the normal and cancer spectra. It permitted us to intuitively visualize which elements contributed to the differences between the two groups.

A significant contribution to the ability to distinguish between healthy and cancerous samples is Ca, whose doublet was observed at 393.37 and 396.85 nm. The intensity of the Ca peaks was stronger in the cancer samples.

Another strong contribution to differentiation was provided by Na, whose peaks were observed at 589.0 nm and 589.6 nm. Their intensities were weaker for the normal samples.

To explore the differences in the relative intensity between elements in normal tissue and cancer samples, each spectrum's intensity was normalized by its highest value.

As observed in Fig. 4, the differences between the groups were difficult to determine solely on the visual examination of the spectra. Thus, chemometric methods were used to classify the spectra. Principal component analysis (PCA) is an unsupervised algorithm that has been successfully used to analyze LIBS data [9]; it aims at combining and replacing the original variables with a new, smaller set of features (principal components) while losing as little information as possible. PCA is commonly used to reduce the dimensions of the data.

This is especially useful with LIBS data, as each spectrum is composed of thousands of intensity values. The PCA results can be displayed using the scores, which are values describing the variation in the samples for each principal component. The scores for the two principal components that express most of the variation in the data set are used for a scatter plot, which gives a visual indication of whether the samples separate into distinguishable clusters.

The PCA score plots for the data sets with 10 μs and 2 μs delays are shown in Fig. 5. Although the samples tended to group together, the data points for cancerous and normal tissue did not separate into clearly discrete clusters and did not permit clear visual discrimination; therefore, further analysis was necessary to classify the samples.
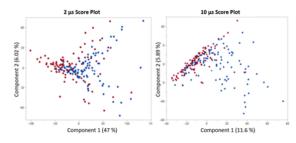

Figure 5. Principal component analysis score plots for time delays of 2 μs (left pabel) and 10 μs (right panel).

Neural networks have been used successfully as a classification method for LIBS data in the past [10, 11]. In

this case, a single-layer perceptron with three hidden nodes was used, with the first 20 principal components from the PC analysis as inputs. For validation purposes, a five-fold methodology was used. This partitioned the dataset into five equal sets and used one for validation, while the other four were used to train the model. This procedure was repeated for each of the five folds, and the model that resulted in the best classification statistics was selected. JMP version 15 (SAS Institute Inc. Cary, North Carolina, USA) was used to perform all statistical analyses.

Table 1. Performance of the neural analysis model applied to the sets of LIBS data with 2 μs and 10 μs delay. (RMSE: Root Mean Square Error)

Training set			
2 μm delay		10 μm delay	
R^2	0.936	R^2	0.260
RMSE	0.141	RMSE	0.445
Misclassification Rate	0.018	Misclassification Rate	0.268
Validation set			
2 μm delay		10 μm delay	
R^2	0.971	R^2	0.478
RMSE	0.099	RMSE	0.387
Misclassification Rate	0.025	Misclassification Rate	0.190

Some of the measures of fitness for the neural network models are shown in Table 1. R^2 is a correlation coefficient that compares the fitness of the model to that of a constant model, with a value of 1 for a perfect model. The R^2 of 0.97 achieved with a 2 μs delay indicates a good correlation between the predicted values calculated by the model and the LIBS data and is considerably higher than the 0.47 obtained with a 10 μs delay. The neural network model using a shorter delay also shows a smaller root mean squared error (RMSE), which translates into an overall lower misclassification rate.

VI. CONCLUSIONS

Detection using LIBS spectra with a time delay of 10 μs allowed obtaining clean spectra with minimal electronic background, similar to those reported in the literature.

Neural network analysis had a prediction rate of 0.732. Using a time delay of 2 μs resulted in spectra containing visible electronic background, which is usually undesirable for spectral analysis. Nonetheless, in this case, the electronic background seemed to offer an unexpected benefit for the neural network's classification accuracy, resulting in a prediction rate of 0.975. These results require further inquiry to unfold the underlying mechanisms, but if confirmed, they could provide a useful approach when using LIBS for the classification of complex biological samples.

All in all, we can say that LIBS, coupled with chemometric and machine learning methods, has the potential to be developed into a minimally invasive technique for prostate cancer detection thanks to the negligible sample size required, the immediacy of the analysis, and the relatively low cost of the required equipment.

REFERENCES

[1] D. Santos Jr, L. C. Nunes, G. G. A. de Carvalho, M. da Silva Gomes, P. F. de Souza, F.de Oliveira Leme, L. G. C. dos Santos and F. J. Krug, Spectrochim. Ac-ta Part B At. Spectrosc. **71**, 3 (2012).

[2] F. Alvira, T. F. Reyes, L. P. Cabrera, L. M. Osorio, Z. P. Baez and G. V. Bautista, Appl. Optics **54**, 4453 (2015).

[3] A. Kumar, F. Y. Yueh, J. P. Singh and S. Burgess, Appl. Optics **43**, 5399 (2004).

[4] N. Noureddine, Y. Markushin, D. C. Conolly, J. Lasue, E. Ewusi-Annan and S. Makrogiannis, Spectrochim. Acta Part B At. Spectrosc. **123**, 33 (2016).

[5] J. Guezenoc, A. Gallet-Budynek and B. Bousquet, Spectrochim. Acta Part B At. Spectrosc. **160**, 105688 (2019).

[6] R. Gaudiuso, E. Ewusi-Annan, W. Xia and N. Melikechi, Spectrochim. Acta Part B At. Spectrosc. **171**, 105931 (2020).

[7] R. Arora, R., M. O. Koch, J. N. Eble, T. M. Ulbright, L. Li and L. Cheng, Cancer **100**, 2362 (2004).

[8] M. A. Bjurlin and S. S. Taneja, Curr. Opin. Urol. **24**, 155 (2014).

[9] J. Wang, L. Li, P. Yang, Y. Chen, Y. Zhu, M. Tong, Z. Hao and X. Li, Lasers Med. Sci. **33**, 1381 (2018).

[10] S. Moncayo, S. Manzoor, T. Ugidos, F. Navarro-Villoslada and J. O. Caceres, Spectrochim. Acta Part B At. Spectrosc. **101**, 21 (2014).

[11] S. Manzoor, S. Moncayo, F. Navarro-Villoslada, J. A. Ayala, R. Izquierdo-Hornillos, F.J. M. de Villena and J. O. Caceres, Talanta **121**, 65 (2014).